Journal of Catalysis 256 (2008) 192–203

Contents lists available at ScienceDirect

Journal of Catalysis

www.elsevier.com/locate/jcat

In situ Raman study on the partial oxidation of methane to synthesis gas over Rh/Al_2O_3 and Ru/Al_2O_3 catalysts

Ying Liu, Fei-Yang Huang, Jian-Mei Li, Wei-Zheng Weng *, Chun-Rong Luo, Mei-Liu Wang, Wen-Sheng Xia, Chuan-Jing Huang, Hui-Lin Wan *

State Key Laboratory of Physical Chemistry of Solid Surfaces and Department of Chemistry, College of Chemistry and Chemical Engineering, Xiamen University, Xiamen, 361005, China

ARTICLE INFO

Article history:
Received 25 December 2007
Revised 11 March 2008
Accepted 13 March 2008
Available online 25 April 2008

Keywords:
Methane partial oxidation
Synthesis gas
Rh/Al_2O_3
Ru/Al_2O_3
In situ Raman
In situ X-ray powder diffraction
Reaction mechanism

ABSTRACT

In situ microprobe Raman and XRD techniques were used to follow the oxidation state of Rh/Al_2O_3 and Ru/Al_2O_3 catalysts during the catalytic ignition process of the partial oxidation of methane (POM) to synthesis gas. It was found that the catalyst was in the fully oxidized state before ignition of the POM reaction, and abruptly changed its oxidation state at the temperature at which the POM reaction started. After the POM reaction was ignited, the amount of Rh_2O_3 or RuO_2 in the catalyst at the entrance of the catalyst bed was below the detection level of Raman spectroscopy. Due to the greater M–O bond strength of Ru–O compared with Rh–O, Ru/Al_2O_3 demonstrated a greater tendency to oxidize than Rh/Al_2O_3 under the POM conditions. This factor affects the oxygen coverage on the two catalysts under reaction conditions and consequently affects the pathways of synthesis gas formation.

1. Introduction

Catalytic partial oxidation of methane (POM) over supported metal catalysts is one of the most promising alternatives to the conventional stream-reforming process [1] for synthesis gas production, particularly in chemical plants of medium size [2–4]. The elucidation of the reaction pathways in POM to synthesis gas over supported transition metal catalysts is a major challenge in the study of this reaction [5]. Although numerous attempts have been made to better understand the mechanisms of synthesis gas formation, the reaction pathway remains under debate [6–18]. Despite the differences in the reaction mechanisms, it is generally agreed that the products of methane oxidation depend on the type and amount of oxygen species on the catalyst [11–18]. Combustion of CH_4 to CO_2 and H_2O is preferred on a metal oxide or metal surface with high oxygen concentrations [11,12,14–18], whereas reduced metal sites are active for dissociative activation of CH_4 to surface carbon species (CH_x, $x = 0$–3) [12–14,16,19], the first step in the CH_4 partial oxidation to synthesis gas by the direct mechanism. Thus, the reaction pathways of POM to synthesis gas are closely related to the oxidation state of the catalyst under the reaction conditions.

For the POM reaction carried out in a fixed-bed reactor using CH_4 and O_2 in a stoichiometric ratio, O_2 in the feed usually is depleted within a very narrow zone near the entrance of the catalyst bed [20]. As a result, the catalyst in various parts of the reactor may experience different chemical states, and the oxidized metal site is found only at the top of the catalyst bed. By monitoring the structure of the catalysts under reaction conditions (especially at the front end of the catalyst bed, where O_2 is still available), we should be able to distinguish between the two proposed mechanisms for the POM reaction.

Alumina is widely used as a catalyst support in the POM reaction. An earlier investigation of rhodium-on-alumina catalysts calcined at 600 and 900 °C indicated that calcination of Rh/Al_2O_3 at 900 °C may bring about reaction of the rhodium with the alumina support, leading to an appreciable drop in the reducibility of the rhodium species that had reacted with the alumina and consequently affecting the catalyst's performance in the POM reaction [21].

As a continuation of the previous research, here we report a more detailed investigation of the Rh/Al_2O_3 and Ru/Al_2O_3 catalysts under a simulated POM reaction feed, using both *in situ* microprobe Raman and *in situ* XRD techniques. The study focused on the oxidation state of the noble metal species in the catalysts during the catalytic ignition process of the POM reaction and its relationship with the reaction pathways of methane. Some parallel measurements on the SiO_2-supported Rh and Ru catalysts, as well as on pure Rh and Ru metal powders, were performed for comparison. Because this study did not concentrate on the reaction of the active metal (oxide) species with the Al_2O_3, the focus was on catalysts thermally pretreated at 110 and 600 °C. Hopefully,

* Corresponding authors. Fax: +86 592 2183047.
E-mail addresses: wzweng@xmu.edu.cn (W.-Z. Weng), hlwan@xmu.edu.cn (H.-L. Wan).

0021-9517/$ – see front matter
doi:10.1016/j.jcat.2008.03.009

Table 1
BET surface area and metal dispersion of the catalysts

Sample	BET surface area ($m^2\ g^{-1}$)	$M_{red(600)}/M_{total}$* × 100%	Metal dispersion	
			$O/M_{red(600)}$	$CO/M_{red(600)}$
Al_2O_3	249	/	/	/
Al_2O_3-600	182	/	/	/
1 wt% Rh/Al_2O_3-110	231	87.4[a]	0.91	1.2
3 wt% Rh/Al_2O_3-110	219	97.2[a]	0.52	0.72
1 wt% Rh/Al_2O_3-600	184	59.8[a]	1.1	1.3
3 wt% Rh/Al_2O_3-600	186	80.9[a]	0.69	0.93
1 wt% Ru/Al_2O_3-110	231	89.2[a]	0.75	0.70
3.7 wt% Ru/Al_2O_3-110	215	>99.0[a]	0.31	0.32
1 wt% Ru/Al_2O_3-600	186	85.6[b]	0.05	0.02
3.7 wt% Ru/Al_2O_3-600	164	96.3[b]	0.02	0.01
SiO_2-600	491	/	/	/
1 wt% Rh/SiO_2-600	488	~100[a]	0.35	0.23
1 wt% Ru/SiO_2-600	495	~100[b]	0.04	0.02

* $M_{red(600)}/M_{total}$: Fraction of the metal species reducible by H_2 at temperature below 600 °C. The data were calculated based on the H_2-TPR profiles of:
[a] re-oxidized, and
[b] fresh catalysts.

this investigation will provide insight into the mechanisms of POM for synthesizing gas over supported noble metal catalysts.

2. Experimental

2.1. Catalyst preparation

The Al_2O_3- and SiO_2-supported noble metal catalysts with the metal loadings specified in Table 1 were prepared by the impregnation method using an aqueous solution of $RhCl_3 \bullet nH_2O$ or $RuCl_3 \bullet nH_2O$ (Sino-Platinum Metals Co. Ltd.). The concentration of the noble metal in the solution was determined by the inductively coupled plasma (ICP) method. To ensure that all of the metal salt was taken up by the support during the impregnation, the noble metal solution containing the required amount of Rh or Ru was diluted with distilled water to a volume beyond which the impregnated catalyst began to appear wet. The Al_2O_3 (TL-02, 60–80 mesh, ~250 m^2/g, Guizhou Alumina Factory, China) and SiO_2 (Aldrich 60A, 60–80 mesh, ~490 m^2/g) supports were calcined at 400 °C for 4 h before use. After water was evaporated, the Al_2O_3 supported catalyst was divided into two parts. The first part of the sample was dried at 110 °C (designated M/Al_2O_3-110, M = Rh or Ru), and the second part was calcined at 600 °C in air for 4 h (designated M/Al_2O_3-600, M = Rh or Ru). All of the SiO_2 supported catalysts were calcined at 600 °C in air for 4 h (designated M/SiO_2-600, M = Rh and Ru).

2.2. Catalytic performance

The catalytic performance of the catalysts was studied using a $CH_4/O_2/Ar = 2/1/45$ mixture (volume ratio) as a reaction feed. The reaction was carried out in a fixed-bed quartz tube reactor (5 mm i.d.) at atmospheric pressure. The catalyst (15.0 mg) was reduced with H_2 at 400 °C (for Ru/Al_2O_3-110) or 600 °C (for Ru/Al_2O_3-600, Rh/Al_2O_3-110, Rh/Al_2O_3-600, and SiO_2-supported catalysts) for 30 min before switching to the reaction feed at room temperature. The temperature of the furnace was then raised from room temperature to 600 °C at a rate of 10 °C/min. During this process, the performance of the catalyst was evaluated at selected temperatures. The products were analyzed by an online gas chromatograph equipped with a thermal conductivity detector (TCD) using Ar (99.999%) as the carrier gas and a carbon sieve column (1.5 m) for the separation of CH_4, O_2, H_2, CO, and CO_2. The conversion of CH_4 (X_{CH_4}) and the selectivities of CO (S_{CO}) and H_2 (S_{H_2}) were calculated based on the following equations:

$$X_{CH_4} = \frac{CH_4(\text{in}) - CH_4(\text{out})}{CH_4(\text{in})} \times 100\%,$$

$$S_{H_2} = \frac{H_2}{2(CH_4(\text{in}) - CH_4(\text{out}))} \times 100\%,$$

$$S_{CO} = \frac{CO}{CO + CO_2} \times 100\%,$$

$$S_{CO_2} = \frac{CO_2}{CO + CO_2} \times 100\%.$$

The pulse reaction of CH_4 was carried out at 600 °C in a fixed-bed quartz tube reactor with 50.0 mg of the supported catalyst or 10 mg of the noble metal oxide powder (made by calcinating $RhCl_3 \bullet nH_2O$ or $RuCl_3 \bullet nH_2O$ powder in air at 600 °C for 4 h) using He containing a few ppm of O_2 as carrier gas. After reduction with H_2 at 600 °C for 30 min, the catalyst was purged with carrier gas (30 mL/min) at the same temperature until the baseline of the mass spectrometer was flat. The CH_4 pulses (99.9%, ~80 μL, at room temperature) were then admitted to the reactor every 6 min. In between the pulses of CH_4, the catalyst was reoxidized by the oxygen present in the carrier gas that was passed continuously through the catalyst bed. The reaction products were analyzed by an online Balzers OmniStar quadrupole mass spectrometer (model QMS 200).

2.3. Catalyst characterization

X-ray powder diffraction (XRD) analysis was carried out by a Panalytical X'pert PRO diffractometer scanning 2θ from 10° to 80°. Cu-$K\alpha$ radiation obtained at 40 kV and 30 mA was used as the X-ray source. The *in situ* XRD experiment was also carried out with the same instrument using a XRK-900 reactor. In each *in situ* XRD experiment, the catalyst sample was first reduced with $H_2/Ar = 5/95$ (volume ratio) at 400 °C (for Ru/Al_2O_3-110) or 600 °C (for Rh/Al_2O_3-110) before switching to the reaction feed ($CH_4/O_2/Ar = 2/1/197$) at room temperature. The temperature of the reactor was then raised from 25 to 750 °C. During this process, the XRD patterns were collected at prespecified temperatures.

The BET surface area of the catalyst was measured by N_2 adsorption at −196 °C using a Micromeritics Tristar 3000 instrument. Before the measurements, the samples were degassed at 300 °C for 2 h. The dispersion of the metal was determined by O_2 and CO chemisorption at 35 °C by assuming O/M and CO/M = 1 stoichiometry. In the experiments, performed using a Micromeritics ASAP 2010 instrument, the catalyst sample (0.4–1.2 g) was first reduced with $H_2/Ar = 5/95$ at 600 °C (or 400 °C for M/Al_2O_3-110 samples) for 30 min, followed by evacuation at 450 °C (or 350 °C for M/Al_2O_3-110 samples) for 30 min. The sample was then cooled to 35 °C under vacuum for O_2 (99.999%) or CO (99.999%) adsorption.

The H_2 temperature-programmed reduction (H_2-TPR) experiments were performed with a GC-TPR apparatus. For each sample, two TPR experiments were performed. The fresh catalyst (0.1 g) was first heated in a flow of $H_2/Ar = 5/95$ mixture (50 mL/min) from 5 to 400 °C (for Ru/Al_2O_3) or 600 °C (for Rh/Al_2O_3, Rh/SiO_2, Ru/SiO_2) at the rate of 10 °C/min to obtain the TPR profile of the fresh catalyst. After reduction with H_2/Ar at 400 or 600 °C for 30 min, the reduced catalyst was reoxidized with an $O_2/Ar = 5/95$ mixture (volume ratio, 20 mL/min) at 400 °C for 30 min, then cooled to 5 °C under O_2/Ar atmosphere. The sample was then purged with a $H_2/Ar = 5/95$ mixture at 5 °C for about 10 min until the baseline was flat. The TPR profile of the reoxidized catalyst was obtained by heating the treated sample from 5 to 900 °C at a rate of 10 °C/min in a flow of a $H_2/Ar = 5/95$ mixture (50 mL/min). The effluent gas mixture was passed through a cold trap at ~−60 °C to remove water. The hydrogen consumption was monitored by a TCD. The results of the second H_2-TPR experiments were also

used to calculate the fraction of the metal species reducible by H_2 below 600 °C ($M_{red(600)}/M_{total}$) in the Rh/Al_2O_3, Ru/Al_2O_3-110, and Rh/SiO_2-600 catalysts. To calculate the fraction of the metal species reducible by H_2 at temperature below 600 °C in the ruthenium catalysts calcined at 600 °C, three additional H_2-TPR experiments (at 5–900 °C) were performed on the fresh Ru/Al_2O_3-600 and Ru/SiO_2-600 catalysts.

The O_2 temperature-programmed desorption (O_2-TPD) experiments were performed with a Micromeritics AutoChem II 2920 instrument. The catalyst (~0.2 g) was first reduced with a $H_2/Ar = 5/95$ mixture at 600 °C for 30 min, followed by oxidation with $O_2/He = 1/4$ (volume ratio) at 500 °C for 30 min and cooling to 20 °C under the same atmosphere. The sample was then purged with He (99.999%) at 20 °C for 30 min, then heated from 20 to 1100 °C at a rate of 10 °C/min in a flow of He (50 mL/min). The O_2 desorption was analyzed with an online ThermoStar quadrupole mass spectrometer (model GSD301T2).

The *in situ* Raman characterization was performed with Renishaw R1000 and Dilor LabRam I microprobe Raman systems equipped with CCD detectors using a home-built high-temperature *in situ* Raman cell designed for the microprobe Raman spectrometer. A diagram of this Raman cell is available elsewhere [21]. The samples were placed in a sample holder equipped with a thermocouple placed below the holder for temperature measurement. The excitation wavelength was a 325-nm He–Cd laser (for Rh/Al_2O_3 catalyst) with a power of ~3 mW or a 632.8-nm He–Ne laser (for Ru/Al_2O_3 catalyst) with a power of ~5 mW measured at the analysis spot. The microscope attachment for the Renishaw R1000 system is based on a Leica DMLM system using an OFR LMU-15×-NUV objective (for a 325-nm laser); that for the Dilor LabRam I is based on an Olympus BX40 system using an Olympus 50× objective (for a 632.8-nm laser). The Raman spectra were measured with 6 cm^{-1} (325 nm) and 4 cm^{-1} (632.8 nm) spectral resolutions. In each experiment, the catalyst sample was first reduced with H_2/Ar (5/95) at 400 °C (for Ru/Al_2O_3-110) or 600 °C (for Ru/Al_2O_3-600 and Rh/Al_2O_3) before switching to the reaction feed ($CH_4/O_2/Ar = 2/1/45$) at room temperature. The temperature of the Raman cell was then raised from room temperature to 600 °C. The Raman spectra of the catalyst were recorded at selected temperatures during this process.

3. Results

3.1. Bulk structure, surface area, and metal dispersion of the catalysts

Fig. 1 shows the XRD patterns of the fresh catalysts. For the Al_2O_3-supported catalysts dried at 110 °C (Rh/Al_2O_3-110 and Ru/Al_2O_3-110) and the Rh/Al_2O_3 catalysts calcined at 600 °C (Rh/Al_2O_3-600), the XRD patterns show only the diffraction peaks due to boehmite (AlO(OH)) (PDF No. 00-021-1307) and/or γ-Al_2O_3 (PDF No. 00-010-0425). For the Ru/Al_2O_3 calcined at 600 °C (Ru/Al_2O_3-600), however, the diffraction pattern of RuO_2 (PDF No. 00-040-1290) also can be observed. For the 1 wt% Rh/SiO_2 catalyst calcined at 600 °C, a broad diffraction peak of high intensity with 2θ at 22.5° and a broad peak of weak intensity with 2θ at about 34° can be seen. The former can be assigned to the diffraction of SiO_2, and the latter may be diffraction lines from the (104) and (110) faces of the Rh_2O_3 (PDF No. 00-042-0541) microcrystals. For the 1 wt% Ru/SiO_2 sample calcined at 600 °C, both diffraction patterns of SiO_2 and RuO_2 (PDF No. 00-040-1290) are clearly visible.

The BET surface areas and metal dispersion data (measured by O_2 and CO chemisorption at 35 °C) of the catalysts are given in Table 1. The surface areas of the catalysts are very close to those of the Al_2O_3 and SiO_2 supports. The metal dispersion data ($O/M_{red(600)}$ and $CO/M_{red(600)}$) given in Table 1 were calibrated with the fractions of the noble metal species in the catalysts reducible by H_2 at temperatures below 600 °C ($M_{red(600)}/M_{total}$), based on the results of H_2-TPR experiments. Compared with the metal dispersion data obtained by O_2 adsorption, CO adsorption was significantly greater over Rh/Al_2O_3 catalysts, with CO/Rh ratios > 1 in some samples, possibly due to the adsorption of CO in the *gem*-dicarbonyl form [22–25]. The metal dispersion of Ru/Al_2O_3 decreased significantly after the catalysts were calcined in air at 600 °C. Comparatively speaking, the dispersion of Rh on Al_2O_3 was not significantly affected by calcination. These findings are consistent with the results of XRD characterization given earlier.

Table 2
Dependence of catalytic performance on the reaction temperature for the Rh/Al_2O_3 catalysts

Catlalysts	Furnace temp. (°C)	Conv. (%)		Sel. (%)			H_2/CO
		CH_4	O_2	CO	H_2	CO_2	
1 wt% Rh/Al_2O_3-600	350	0.8	2.0	0	0	100	/
	400	2.0	6.2	0	0	100	/
	460	8.0	33.3	0	0	100	/
	470	51.9	100	49.3	77.3	50.7	3.1
	500	58.9	100	58.4	79.8	41.6	2.7
	550	71.8	100	76.0	82.1	24.0	2.2
	600	82.6	100	87.7	83.4	12.3	1.9
1 wt% Rh/Al_2O_3-110	350	0.46	2.0	0	0	100	/
	400	1.5	6.9	0	0	100	/
	450	5.7	23.2	0	0	100	/
	460	8.1	32.6	0	0	100	/
	470	52.7	100	49.4	75.8	50.6	3.1
	480	54.5	100	53.0	75.8	47.0	2.9
	500	58.8	100	60.1	78.5	39.9	2.6
	550	71.7	100	76.1	78.2	23.9	2.1
	600	82.5	100	88.4	82.1	11.6	1.9
3 wt% Rh/Al_2O_3-600	350	1.0	3.5	0	0	100	/
	400	2.4	11.6	0	0	100	/
	430	9.7	41.0	0	0	100	/
	440	48.0	100	39.1	74.3	60.9	3.8
	450	49.9	100	43.2	76.1	56.8	3.5
	500	61.0	100	62.3	81.8	37.7	2.6
	550	73.3	100	77.5	82.2	22.5	2.1
	600	84.1	100	88.9	82.4	11.1	1.9
3 wt% Rh/Al_2O_3-110	350	1.2	3.6	0	0	100	/
	400	4.7	18.0	0	0	100	/
	420	8.7	35.2	0	0	100	/
	430	45.7	100	34.5	73.8	65.5	4.3
	440	47.9	100	38.1	73.9	61.9	3.9
	450	49.4	100	41.0	76.0	59.0	3.7
	500	60.6	100	60.3	80.9	39.7	2.7
	550	73.0	100	76.2	81.3	23.8	2.1
	600	84.0	100	88.1	82.4	11.9	1.9

Reaction condition: $CH_4/O_2/Ar = 2/1/45$, $m_{cat.} = 15$ mg, $SV = 2.0 \times 10^5$ $mL\,h^{-1}\,g^{-1}$. Catalysts were reduced with H_2 at 600 °C before testing. Data were collected after 20 min on stream.

3.2. Catalytic performance of the catalysts at different temperatures

Tables 2 and 3 characterize the catalytic performance of the Rh/Al_2O_3 and Ru/Al_2O_3 catalysts at various temperatures during stepwise heating of the previously reduced catalysts under $CH_4/O_2/Ar = 2/1/45$ flow from 30 to 600 °C. For comparison, the catalytic performance of 1 wt% Rh/SiO_2-600 and 1 wt% Ru/SiO_2-600 catalysts is presented in Table 4. For all of the catalysts, three temperature regions can be distinguished from the evolution of CH_4 conversion products (CO_2, CO, and H_2). In the low-temperature region, O_2 in the reactant was not completely consumed. Oxidation of CH_4 over the catalysts started at between 300 and 350 °C, depending on the amount of metal loading, but no CO or H_2 was detected in the product. The CH_4 conversion in this temperature region was low and increased slowly with increasing temperature. In the mid-temperature region (370–530 °C), the POM

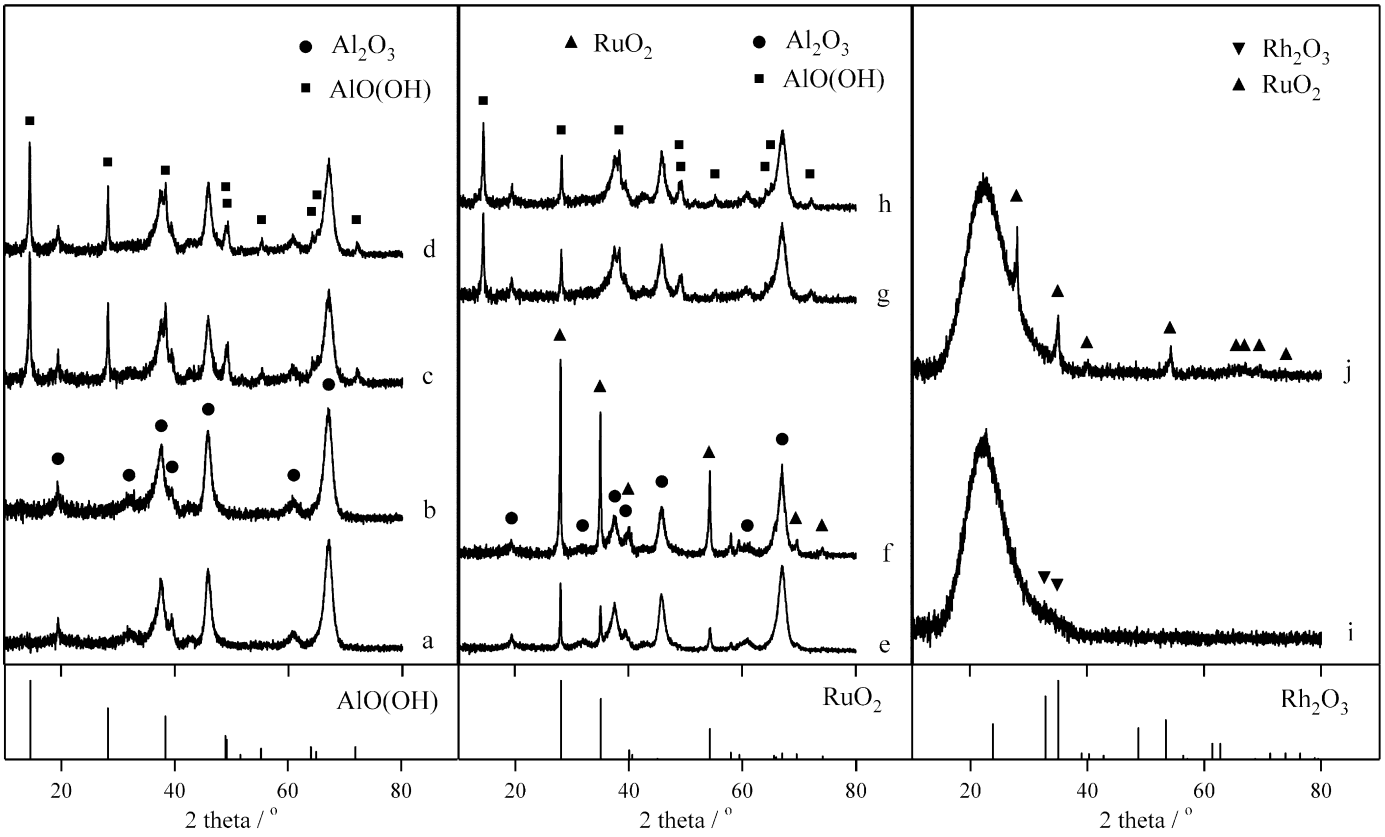

Fig. 1. XRD patterns of the fresh catalysts. **a**. 1 wt% Rh/Al_2O_3-600, **b**. 3 wt% Rh/Al_2O_3-600, **c**. 1 wt% Rh/Al_2O_3-110, **d**. 3 wt% Rh/Al_2O_3-110, **e**. 1 wt% Ru/Al_2O_3-600, **f**. 3.7 wt% Ru/Al_2O_3-600, **g**. 1 wt% Ru/Al_2O_3-110, **h**. 3.7 wt% Ru/Al_2O_3-110, **i**. 1 wt% Rh/SiO_2-600, **j**. 1 wt% Ru/SiO_2-600.

reaction over the catalysts (which can be determined experimentally by the rapid increase in CH_4 and O_2 conversion accompanied by H_2 and CO formation) was seen to ignite. On both Rh/Al_2O_3 and Ru/Al_2O_3, the temperatures required to ignite the POM reaction decreased with increasing metal loading. Similar results have been reported by Wang and Ruckenstein for the POM reaction on Rh/Al_2O_3 catalysts [26]. In the high-temperature region after the POM reaction was ignited, O_2 conversion was close to 100%. The amounts of CO and H_2 produced showed an increasing trend with temperature, whereas the formation of CO_2 exhibited an opposite trend. Moreover, even though the reaction mixture (at $CH_4/O_2 = 2$) used in the experiment had been diluted with a large amount of Ar, the observed CH_4 conversions and CO selectivities for the POM reaction were still higher than the thermodynamic equilibrium values for the reaction reported previously [27] at the temperatures specified in Table 2, indicating that a hot-spot layer still existed in the catalyst bed under the experimental conditions.

As shown in Tables 2 and 3, the temperatures required to ignite the POM reaction on Rh/Al_2O_3 were always lower than those on Ru/Al_2O_3 at comparable metal loadings. A similar phenomenon was observed on the SiO_2-supported catalysts (Table 4). Moreover, for the Rh and Ru catalysts with comparable metal loadings, the temperature required to ignite the POM reaction was much lower on the SiO_2-supported catalyst than that on the Al_2O_3-supported catalyst, indicating a significant influence of the support on the performance of the metal species. The stronger interaction of Rh and Ru with Al_2O_3 compared with SiO_2 should be responsible for the higher POM ignition temperatures on the Al_2O_3-supported catalysts. The much lower interaction of rhodium with SiO_2 is evident from the XRD patterns shown in Fig. 1. The weak diffraction maximum due to Rh_2O_3 seen on the silica support indicates that the Rh/SiO_2-600 catalyst contained larger rhodium particles.

3.3. H_2-TPR and O_2-TPD characterization

H_2-TPR and O_2-TPD were used to investigate the reducibility and the metal–oxygen bond strength of the metal oxide species on the supported metal catalysts. The corresponding results are shown in Figs. 2 and 3. The quantified amounts from the TPR profiles for the catalysts are specified in Table 1. The TPR profiles of Rh/Al_2O_3 are composed of two major reduction bands with temperatures at peak maxima (T_m) of below 110 and above 750 °C, respectively. These bands can be attributed to the reduction of rhodium oxide (mainly amorphous Rh_2O_3) species ($T_m < 110$ °C) with different extent of interaction with Al_2O_3 and the $Rh(AlO_2)_y$ species ($T_m > 750$ °C) formed by diffusion of rhodium oxides into sublayers of Al_2O_3 structure after high-temperature (>500 °C) oxidation [28]. Due to the interaction between Rh and Al_2O_3 [28,29], the fractions of the oxidized Rh species in the Rh/Al_2O_3 catalysts irreducible at temperatures below 600 °C increased significantly in the samples with low (1 wt%) Rh loading as well as in samples calcined at high temperature (600 °C). The position of the low-temperature TPR peak ($T_m = 98$–105 °C) shifted toward the low-temperature direction in the high-Rh loading samples.

The TPR profiles of Ru/Al_2O_3 are composed of one or two relatively sharp low-temperature reduction peaks with T_m of 81–96 and 157–170 °C, respectively, and a broad high temperature reduction band with T_m above 700 °C. According to the literature [30–32], the peaks with T_m around 90 °C can be assigned to the reduction of well-dispersed RuO_x species containing mainly RuO_2, and the peaks with T_m around 160 °C can be attributed to the reduction of bulk RuO_2 species. The broad TPR band with $T_m > 700$ °C may be assigned to the reduction of the oxidized Ru species that interact strongly with Al_2O_3. Similar to the Rh/Al_2O_3 catalysts, the fraction of the oxidized Ru species in the Ru/Al_2O_3 catalysts irreducible by H_2 at temperatures below 600 °C also increased with

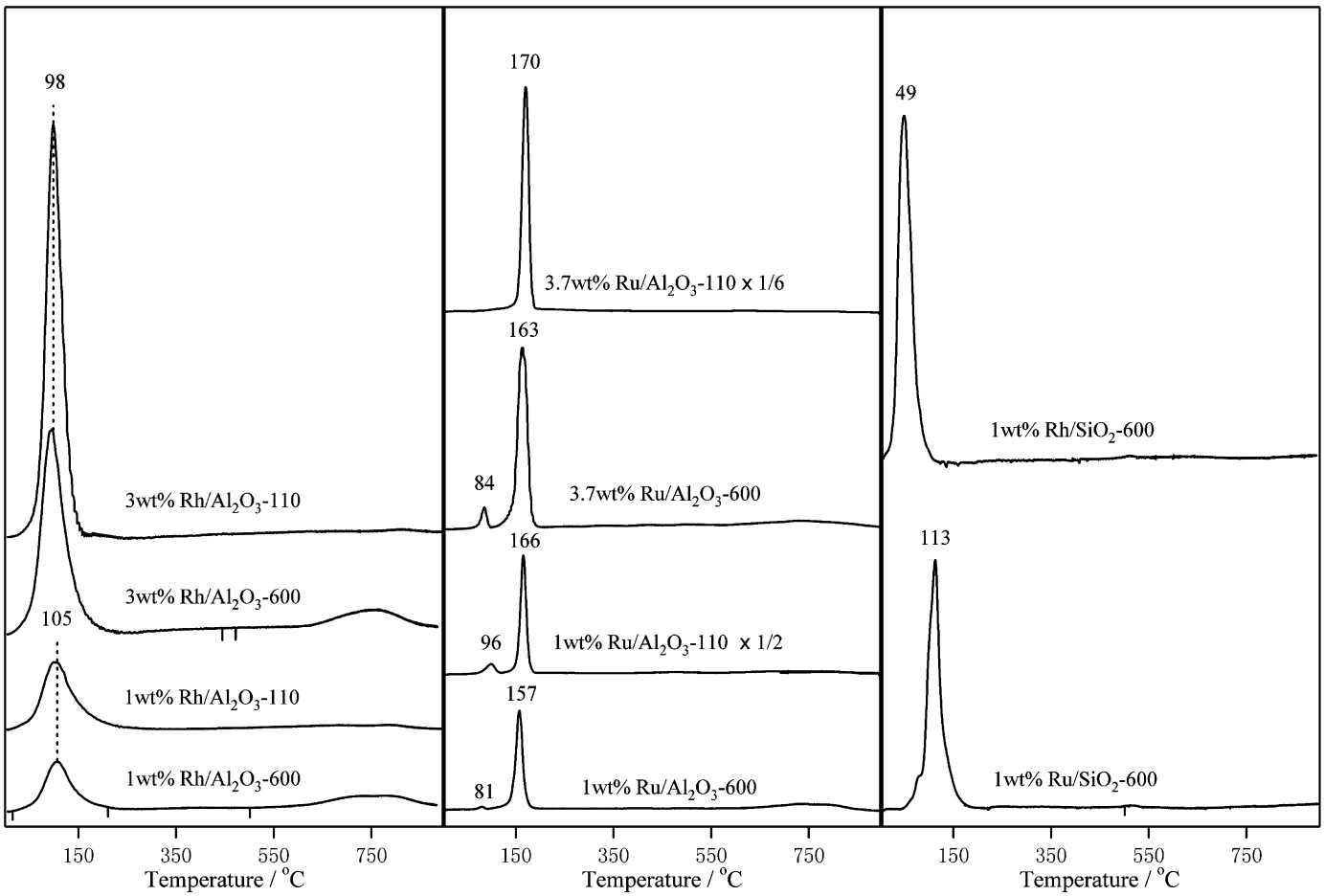

Fig. 2. H_2-TPR profiles of the catalysts. Before the experiment, the catalysts were reduced with $H_2/Ar = 5/95$ mixture at 400 °C (for Ru/Al_2O_3) or 600 °C (for Rh/Al_2O_3) for 30 min followed by oxidation with $O_2/Ar = 5/95$ mixture at 400 °C for 30 min.

increasing calcination temperature and decreased with increasing Ru loading (Table 1). Compared with the TPR profiles of Ru/Al_2O_3-110, the intensities of the TPR signals for Ru/Al_2O_3-600 were significantly lower, possibly because of the significantly smaller particle size of the ruthenium species in the former catalyst. As demonstrated by the metal dispersion data in Table 1, the particle size of the ruthenium species in Ru/Al_2O_3 increased significantly after calcination at 600 °C. Because larger metallic Ru particles better preserve their metallic state compared with well-dispersed species [33], only the surface of large metallic Ru particles in Ru/Al_2O_3-600 are oxidized during the process of reoxidation treatment before the TPR experiment, whereas most of the small metallic Ru particles in Ru/Al_2O_3-110 can be converted to RuO_2 by reoxidation at 400 °C. For the SiO_2-supported catalysts, TPR peaks with T_m at 49 and 113 °C were observed on 1 wt% Rh/SiO_2-600 and 1 wt% Ru/SiO_2-600, respectively, and no reduction peak was observed in the high-temperature region. Compared with the Al_2O_3-supported Rh and Ru catalysts, reduction of the Rh_2O_3 and RuO_2 species on SiO_2 occurred at lower temperatures, also due to the weaker interaction of Rh and Ru with SiO_2.

Fig. 3 shows the O_2-TPD profiles of the Al_2O_3- and SiO_2-supported Rh and Ru catalysts. The O_2-TPD profiles of Rh/Al_2O_3-600 and Rh/SiO_2-600 consist of two O_2 desorption peaks with maxima at 880, 985 °C and 820, 860 °C, respectively, attributable to two kinds of rhodium oxide species in the samples. Based on our previous O_2-TPD and H_2-TPR characterizations on Rh/Al_2O_3 and Rh/SiO_2 catalysts [21], the O_2 desorption peaks for the Rh catalysts shown in Fig. 3 can be assigned to the decomposition of the rhodium oxide species reducible by H_2 at temperatures below 600 °C. Due to the strong interaction between rhodium oxide species and Al_2O_3, the O_2 desorption temperatures on Rh/Al_2O_3-600 (880, 985 °C) were significantly higher than those on Rh/SiO_2-600 (820, 860 °C), in agreement with the results of H_2-TPR experiments presented earlier. The O_2-TPD profile of Ru/Al_2O_3-600 or Ru/SiO_2-600 comprises only a single desorption peak with T_m above 1024 °C. Compared with the Rh catalysts, the O_2 desorption temperatures on Ru/Al_2O_3-600 and Ru/SiO_2-600 are very close, possibly due to the weaker interaction between RuO_2 and Al_2O_3 compared with that between Rh_2O_3 and Al_2O_3.

3.4. High-temperature in situ Raman and XRD characterizations

In situ Raman and *in situ* XRD measurements were performed to gain insight into the chemical states of the noble metal species in the catalyst during the catalytic ignition process of POM reaction and its relationship with the performance of the catalysts characterized in Tables 2 and 3. In these experiments, *in situ* Raman spectroscopy was used to monitor the oxidation state of the noble metal species in the catalysts located at the entrance of catalyst bed, whereas *in situ* XRD was used to analyze the bulk structure of the catalysts during the catalytic ignition process of the POM reaction.

Fig. 4 shows the Raman spectra of 3 wt% Rh/Al_2O_3-600 and 3.7 wt% Ru/Al_2O_3-600 catalysts recorded at 600 °C under O_2, $H_2/Ar = 5/95$, and a simulated POM feed with $CH_4/O_2/Ar = 2/1/45$. In the spectra recorded under O_2 (Fig. 4a), a broad band with maximum at ~550 cm^{-1} corresponding to amorphous Rh_2O_3 [34] was observed on 3 wt% Rh/Al_2O_3-600, and two relatively sharp

Table 3
Dependence of catalytic performance on the reaction temperature for the Ru/Al_2O_3 catalysts

Catlalysts	Furnace temp. (°C)	Conv. (%)		Sel. (%)			H_2/CO
		CH_4	O_2	CO	H_2	CO_2	
1 wt% Ru/Al_2O_3-600	300	0.44	1.8	0	0	100	/
	350	0.65	2.8	0	0	100	/
	400	1.9	7.4	0	0	100	/
	450	4.8	20.0	0	0	100	/
	500	11.2	46.1	0	0	100	/
	520	16.2	65.2	0	0	100	/
	530	62.0	100	64.3	80.7	35.7	2.5
	550	68.9	100	73.1	82.0	26.0	2.2
	600	80.9	100	85.9	82.5	14.1	1.9
1 wt% Ru/Al_2O_3-110	300	0	0	0	0	0	/
	350	0.83	3.2	0	0	100	/
	400	2.3	8.2	0	0	100	/
	450	7.7	28.5	0	0	100	/
	500	17.7	71.8	0	0	100	/
	510	58.2	100	56.8	79.9	43.1	2.8
	550	71.1	100	75.2	83.0	24.8	2.2
	600	82.5	100	87.5	83.0	12.5	1.9
3.7 wt% Ru/Al_2O_3-600	300	0.74	2.5	0	0	100	/
	350	1.6	6.4	0	0	100	/
	400	4.1	16.5	0	0	100	/
	450	10.4	43.8	0	0	100	/
	470	16.1	64.9	0	0	100	/
	480	50.2	100	43.9	76.6	56.1	3.5
	500	56.9	100	55.1	80.5	44.9	2.9
	550	71.3	100	75.1	82.3	24.9	2.2
	600	82.8	100	87.8	82.4	12.2	1.9
3.7wt% Ru/Al_2O_3-110	300	1.0	3.8	0	0	100	/
	350	2.6	11.3	0	0	100	/
	400	7.3	29.2	0	0	100	/
	450	22.3	89.0	0	0	100	/
	460	44.9	100	35.3	71.9	64.7	4.07
	500	59.	100	57.3	81.3	42.7	2.84
	550	72.4	100	76.9	82.4	23.1	2.14
	600	83.9	100	88.7	82.1	11.3	1.85

Reaction condition: $CH_4/O_2/Ar = 2/1/45$, $m_{cat.} = 15$ mg, $SV = 1.2 \times 10^5$ mL h^{-1} g^{-1}. Catalysts were reduced with H_2 at 400 °C (for Ru/Al_2O_3-110) and 600 °C (for Ru/Al_2O_3-600), respectively, before testing. Data were collected after 20 min on stream.

bands at 504 and 618 cm^{-1} corresponding to RuO_2 [35] were observed on 3.7 wt% Ru/Al_2O_3-600. These bands disappeared within 2 min when the O_2-pretreated samples were switched to a flow of $H_2/Ar = 5/95$ mixture at 600 °C (Fig. 4b). It is interesting that the Raman spectra of the catalysts recorded at 600 °C under a simulated POM feed (Fig. 4c) were very similar to those recorded under the H_2/Ar atmosphere. No Raman bands belonging to Rh_2O_3 or RuO_2 species were detected. These findings indicate that most of the noble metal species in the catalysts located at the entrance of the catalyst bed were in the metallic state under the condition when the POM reaction occurred with CH_4 conversion >82% and CO selectivity >87% (Tables 2 and 3).

Figs. 5 and 6 show the Raman spectra of the Rh/Al_2O_3-110 and Ru/Al_2O_3-110 catalysts recorded at specified temperatures under a $CH_4/O_2/Ar = 2/1/45$ atmosphere as the temperature of the Raman cell was raised from 30 to 550 or 600 °C. As soon as the H_2-prereduced Rh/Al_2O_3-110 or Ru/Al_2O_3-110 catalyst was switched to $CH_4/O_2/Ar$ at room temperature, Raman bands of the corresponding noble metal oxides (Rh_2O_3 or RuO_2) species appeared, indicating that metallic rhodium or ruthenium species in the catalyst (at least those on the surface of the metal particles) can be oxidized by O_2 in the reactant even at room temperature. As the temperature of the samples increased, the Raman band of Rh_2O_3 species (553 cm^{-1}) on 1 wt% Rh/Al_2O_3-110 and 3 wt% Rh/Al_2O_3-110 disappeared at 470 and 440 °C, respectively, whereas the Raman bands of RuO_2 species (504 and 618 cm^{-1}) on 1 wt% Ru/Al_2O_3-110 and 3.7 wt% Ru/Al_2O_3-110 disappeared at 500 and 470 °C, respectively. Interestingly, the temperatures at which the noble metal oxide species in the catalysts vanished were in good agreement with the temperatures at which the POM reaction over the catalysts ignited (see Tables 2 and 3). Similar phenomena were observed on the Rh/Al_2O_3-600 and Ru/Al_2O_3-600 catalysts (spectra not shown). No other species were detected by Raman spectroscopy on either the Rh/Al_2O_3 or Ru/Al_2O_3 samples.

Figs. 7 and 8 show XRD patterns of the Rh/Al_2O_3-110 and Ru/Al_2O_3-110 catalysts recorded under a flow of a $CH_4/O_2/Ar = 2/1/197$ mixture (80 mL/min) during the stepwise heating of the

Table 4
Dependence of catalytic performance on the reaction temperature for the Rh/SiO_2 and Ru/SiO_2 catalysts

Catlalysts	Furnace temp. (°C)	Conv. (%)		Sel. (%)			H_2/CO
		CH_4	O_2	CO	H_2	CO_2	
1 wt% Rh/SiO_2-600	300	2.5	8.3	0	0	100	/
	350	11.6	45.9	0	0	100	/
	360	22.2	89.2	0	2.3	100	/
	370	25.0	97.5	4.2	7.6	95.8	3.7
	400	29.2	100	16.7	26.4	83.3	3.2
	450	39.0	100	41.3	53.4	58.7	2.6
	500	53.1	100	59.0	72.1	41.0	2.4
	550	68.0	100	75.5	82.9	24.5	2.2
	600	81.6	100	87.7	84.6	12.3	1.9
1 wt% Ru/SiO_2-600	300	0	0	0	0	0	/
	350	0.77	2.4	0	0	100	/
	400	3.4	10.5	0	0	100	/
	440	9.9	39.7	0	0.23	100	/
	450	37.0	100	20.2	56.8	79.8	5.6
	500	47.7	100	41.7	71.9	58.3	3.4
	550	60.7	100	64.4	78.3	35.6	2.4
	600	72.1	100	79.4	79.7	20.6	2.0

Reaction condition: $CH_4/O_2/Ar = 2/1/45$, $m_{cat.} = 15$ mg, $SV = 2.0 \times 10^5$ mL h^{-1} g^{-1}. Catalysts were reduced with H_2 at 600 °C before testing. Data were collected after 20 min on stream.

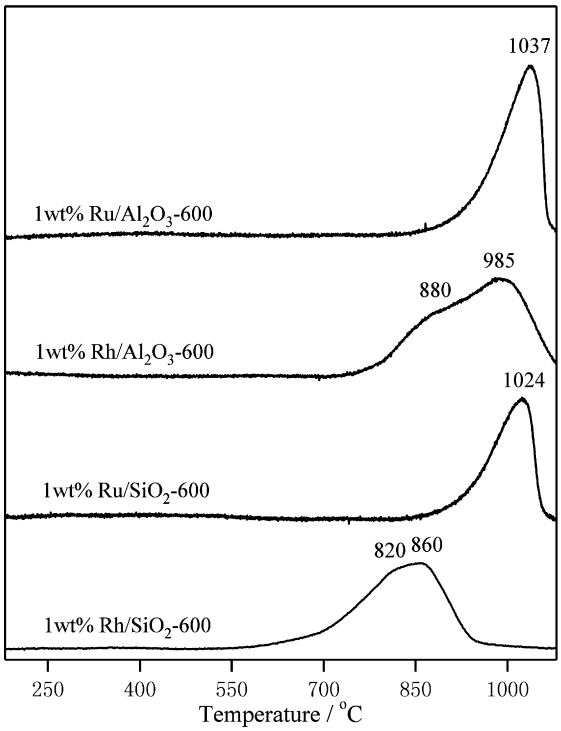

Fig. 3. O_2-TPD profiles of the catalysts. Before the experiment, the catalysts were reduced with $H_2/Ar = 5/95$ mixture at 600 °C for 30 min followed by oxidation with $O_2/He = 1/4$ mixture at 500 °C for 30 min.

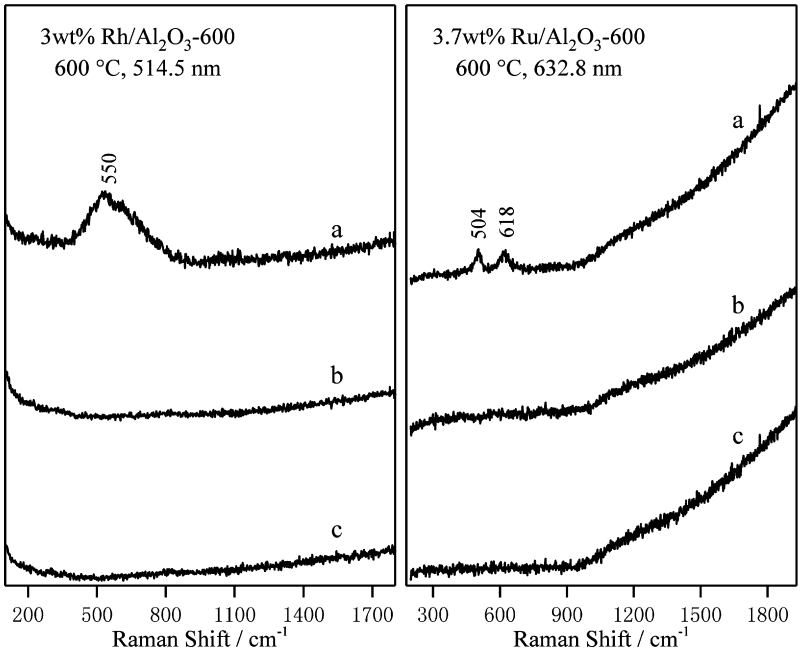

Fig. 4. Raman spectra of 3 wt% Rh/Al_2O_3-600 and 3.7 wt% Ru/Al_2O_3-600 catalysts recorded at 600 °C under **a**. O_2, **b**. $H_2/Ar = 5/95$, and **c**. $CH_4/O_2/Ar = 2/1/45$.

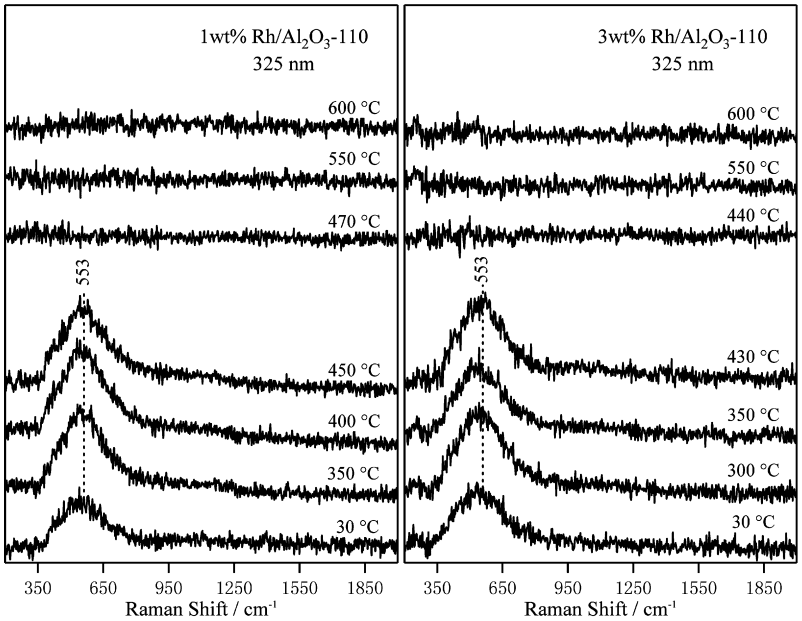

Fig. 5. Raman spectra of 1 wt% Rh/Al_2O_3-110 and 3 wt% Rh/Al_2O_3-110 catalysts recorded at the indicated temperature during stepwise heating of the previously reduced samples under $CH_4/O_2/Ar = 2/1/45$ atmosphere from room temperature to 600 °C. The Raman spectra of Al_2O_3 support were subtracted. Before switching to $CH_4/O_2/Ar$ mixture, the catalysts were reduced with $H_2/Ar = 5/95$ mixture at 600 °C for 30 min.

H_2-prereduced samples from 25 to 750 °C in the XRK-900 reactor. Similar to the XRD patterns of fresh Rh/Al_2O_3 catalysts, no characteristic diffraction peaks due to the rhodium oxide or metallic Rh species were detected on the Rh/Al_2O_3-110 catalysts over the entire temperature range, indicating high dispersion of rhodium species on the Al_2O_3 support.

For the Ru/Al_2O_3-110 catalysts under a $CH_4/O_2/Ar$ mixture, no diffraction patterns due to RuO_2 or Ru species were detected at temperatures below 200 °C. When the temperature of the reactor was raised to 300–450 °C, diffraction peaks of crystalline RuO_2 phase ($2\theta = 28.0$, 35.1 and 54.3°) were observed, with intensities increasing with temperature. These results suggest that the metallic ruthenium species in the catalysts were extensively oxidized by O_2 in the reactant in this temperature range. In addition, the aggregation of the oxidized RuO_2 species to larger RuO_2 particles also may have occurred when the Ru/Al_2O_3-110 samples were heated under the reaction mixture to above 300 °C, as evidenced by the increased intensity of the XRD peaks of RuO_2 with increasing temperature. With a further rise in the temperature, the XRD peaks of RuO_2 over 1 wt% Ru/Al_2O_3-110 and 3.7 wt% Ru/Al_2O_3-110 vanished at 500 and 450 °C, respectively, and the characteristic diffraction peaks of metallic Ru phase were detected. Similar to the results of *in situ* Raman characterization presented earlier, the temperatures at which the RuO_2 species in the catalysts disappeared also were in good agreement with the temperatures at which the POM reaction over the catalysts ignited.

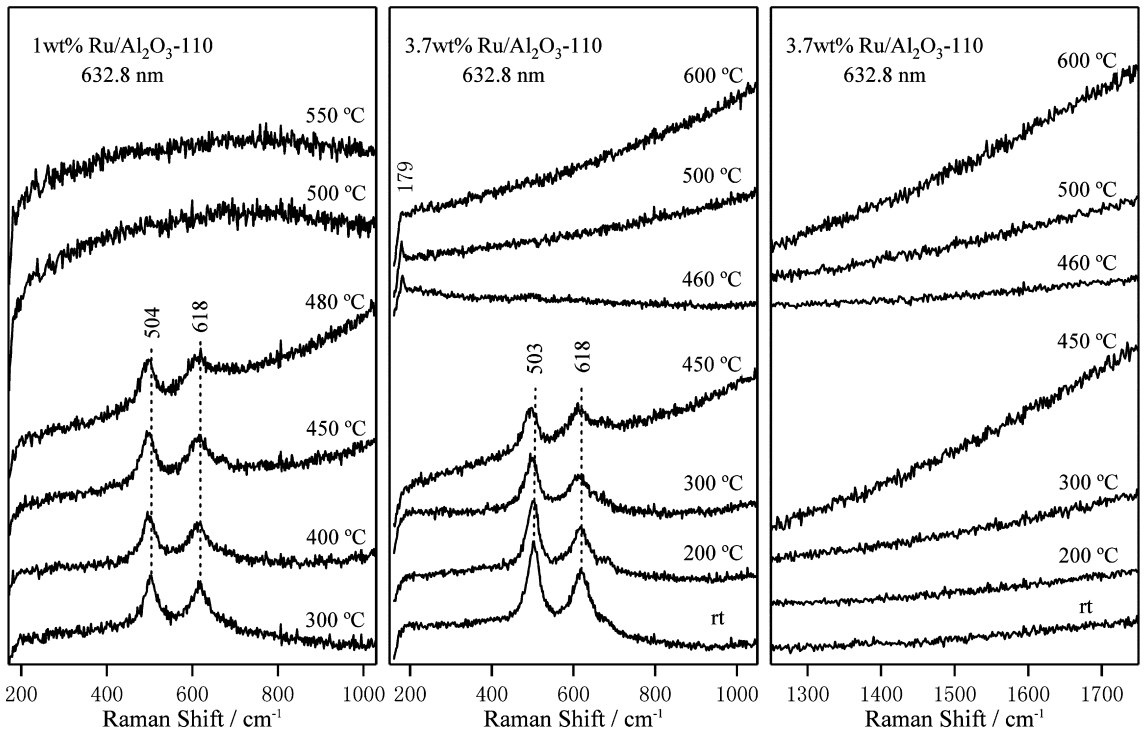

Fig. 6. Raman spectra of 1 wt% Ru/Al_2O_3-110 and 3.7 wt% Ru/Al_2O_3-110 recorded at the indicated temperature during stepwise heating of the previously reduced samples under $CH_4/O_2/Ar = 2/1/45$ atmosphere from room temperature to 600 °C. Before switching to $CH_4/O_2/Ar$ mixture, the catalysts were reduced with $H_2/Ar = 5/95$ mixture at 400 °C for 30 min.

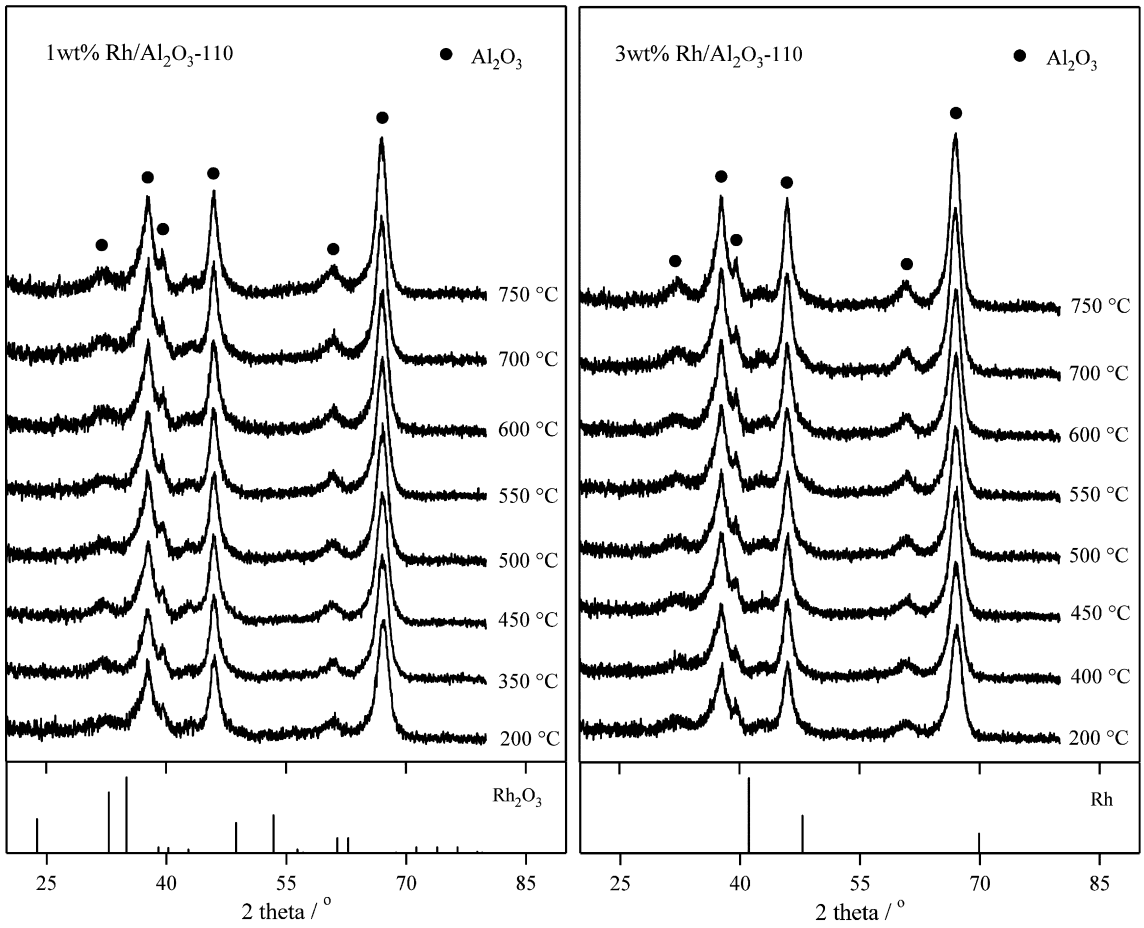

Fig. 7. XRD patterns of 1 wt% Rh/Al_2O_3-110 and 3 wt% Rh/Al_2O_3-110 catalysts recorded at the indicated temperature during stepwise heating of the previously reduced samples under a flow of $CH_4/O_2/Ar = 2/1/197$ (80 mL/min) from 30 to 750 °C. Before switching to $CH_4/O_2/Ar$ mixture, the catalysts were reduced with $H_2/Ar = 5/95$ mixture at 600 °C for 30 min.

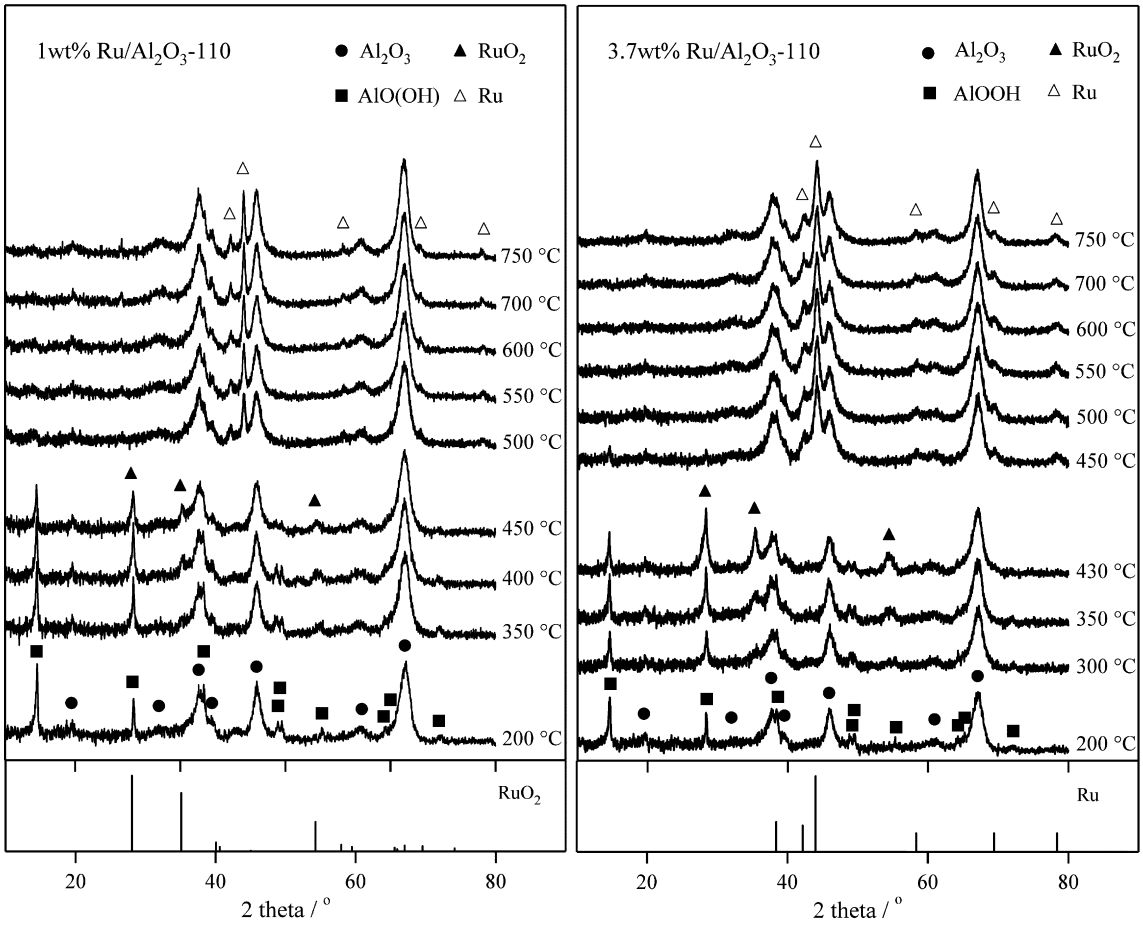

Fig. 8. XRD patterns of 1 wt% Ru/Al_2O_3-110 and 3.7 wt% Ru/Al_2O_3-110 catalysts recorded at the indicated temperature during stepwise heating of the previously reduced samples under a flow of $CH_4/O_2/Ar = 2/1/197$ (80 mL/min) from 30 to 750 °C. Before switching to $CH_4/O_2/Ar$ mixture, the catalysts were reduced with $H_2/Ar = 5/95$ mixture at 400 °C for 30 min.

3.5. Pulse reaction of CH_4 over the catalysts

For both SiO_2- and Al_2O_3-supported catalysts with comparable amounts of noble metal loading, the temperatures required to ignite the POM reaction were always lower on the Rh catalysts than on the Ru catalysts. The results of *in situ* Raman and XRD characterizations suggest that reduction of the RuO_2 species was more difficult than reduction of the Rh_2O_3 species under the POM reaction atmosphere. To further elucidate the relationship between the redox properties of the noble metal species and performance in the POM reaction, CH_4-pulse experiments were performed over Ru and Rh metal powders, as well as over the Al_2O_3-supported catalysts. The experiments were performed using He containing a few ppm of O_2 as the carrier gas; the results are shown in Fig. 9. When pulses of CH_4 were introduced to the H_2-prereduced Ru metal or the supported Ru catalysts at 6-min intervals, the completely oxidized product, CO_2, could be detected in every pulse. In contrast, CO_2 was formed only in the first two pulses (and never thereafter) when CH_4 was pulsed over the supported Rh catalysts, and no CO_2 was detected in the product for the pulse reaction over the H_2-prereduced Rh metal. Combustion of CH_4 to CO_2 and H_2O was favored on the catalysts with high surface oxygen concentrations [14–18]. On the other hand, at a sufficiently low surface oxygen concentration on the catalyst, CH_4 can be selectively converted to CO [15,17]. Thus, the results of CH_4 pulse reaction over the catalysts can be plausibly related to the significantly higher surface oxygen concentrations on the ruthenium catalysts than on the rhodium catalysts. These results indicate that metallic Ru demonstrated a greater tendency toward oxidation than metallic Rh under the experimental conditions.

4. Discussion

4.1. Chemical state of the noble metal species in the Rh/Al_2O_3 and Ru/Al_2O_3 catalysts before ignition of the POM reaction

When a H_2-prereduced sample is heated under a CH_4/O_2 mixture at the POM stoichiometric ratio from 25 to 600 or 750 °C, the oxidation state of the metal species in the catalyst is determined mainly by the relative rates of two competitive reactions at the different temperatures, that is, the oxidation of metal species by O_2 to the corresponding metal oxide [Eq. (1)] and the reduction of the metal oxide species by CH_4 to the corresponding metal [Eq. (2)],

$$xM + \frac{y}{2}O_2 \rightarrow M_xO_y \quad (1)$$

and

$$M_xO_y + \frac{y}{4}CH_4 \rightarrow \frac{y}{4}CO_2 + \frac{y}{2}H_2O + xM \quad (M = Rh, Ru). \quad (2)$$

The results of *in situ* Raman characterization (Figs. 5 and 6) clearly indicate that when a H_2-prereduced catalyst was switched to the $CH_4/O_2/Ar = 2/1/45$ mixture at room temperature, the surface of the Rh and Ru particles located at the front end of the catalyst bed were readily oxidized by O_2 in the feed, as demonstrated by the bands of Rh_2O_3 (~550 cm^{-1}) and RuO_2 (503, 618 cm^{-1}) species in the corresponding Raman spectra. Considering the very

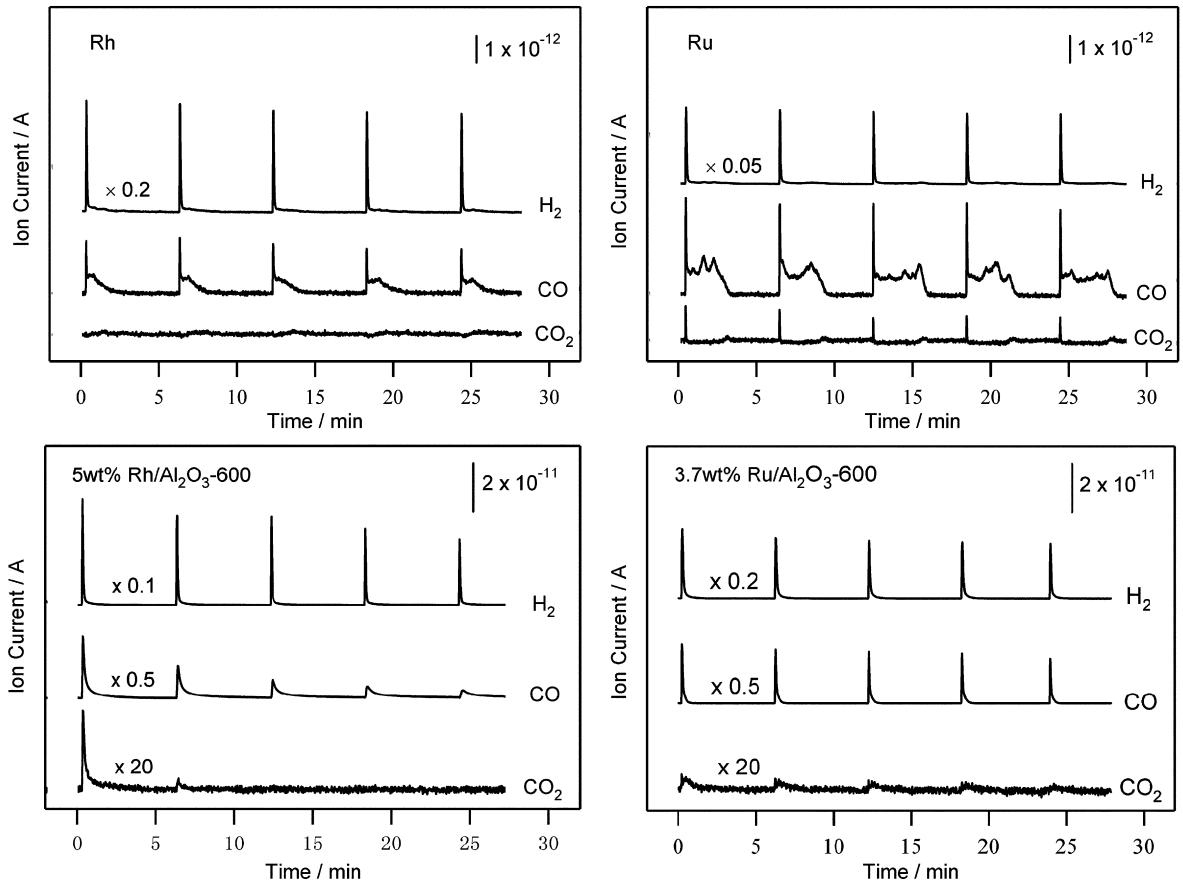

Fig. 9. CO and CO_2 formations by pulsing CH_4 over Rh and Ru metals as well as over 5 wt% Rh/Al_2O_3-600 and 3.7 wt% Ru/Al_2O_3-600 catalysts at 600 °C using He containing a trace amount of O_2 as a carrier gas. The catalysts were pre-reduced with H_2 at 600 °C.

low catalyst activity and O_2 conversion at room temperature, it is reasonable to conclude that O_2 in the reactant should be capable of oxidizing the surface of the noble metal particles in the entire catalyst bed.

The corresponding *in situ* XRD patterns recorded at temperatures below 200 °C exhibited only the diffraction peaks of γ-Al_2O_3 and AlOOH. The absence of any detectable noble metal or oxide peaks in the XRD patterns of Rh/Al_2O_3-110 and Ru/Al_2O_3-110 recorded at temperatures below 200 °C suggests that both metallic and oxidized Rh and Ru species were well dispersed on the support and that the average crystallite size of the noble metal species in the catalysts was below the limit of detection by XRD.

Sintering of the rhodium species in the Rh/Al_2O_3 catalyst at high temperature was not significant, because of the strong interaction of rhodium oxide with the surface of the alumina support [21,28,29]. Consequently, the *in situ* XRD analysis provided no information on the structure of the rhodium species (oxide or metal) in the catalyst during catalytic ignition of the POM reaction. However, combined with the results of *in situ* Raman characterization shown in Fig. 5 (indicating that metallic rhodium species in Rh/Al_2O_3 could be oxidized by O_2 in the reactant even at room temperature) and the results of the catalytic performance test given in Table 2 (indicating <40% O_2 conversion in the reaction feed even when the furnace temperature was only 10 °C below the POM ignition temperature), it is reasonable to conclude that the rhodium species in the catalyst bed (at least those on the surface of rhodium particles) are also in the oxidized state before ignition of the POM reaction. This conclusion is also in agreement with the results of *in situ* X-ray absorption fine structure (XAFS) [36] and *in situ* X-ray absorption near-edge structure (XANES) [37] studies on the Rh/Al_2O_3 catalyst under $CH_4/O_2/He$ (6/3/91) reaction mixture reported by Grunwaldt et al. Both of these results indicate that the rhodium species in the catalyst were in the oxidized state before ignition of the POM reaction. A weight increase due to the oxidation of metallic rhodium to rhodium oxide was observed when a prereduced Rh/γ-Al_2O_3 catalyst was heated at 350 °C in a flow of $CH_4/O_2/Ar$ (2/1/20.5) [38].

On heating the Ru/Al_2O_3-110 catalysts under the $CH_4/O_2/Ar$ reaction mixture from 200 °C to the temperature of ignition of the POM reaction, the XRD pattern of bulk RuO_2 was detected (Fig. 8), indicating that metallic ruthenium species in the catalysts were extensively oxidized to RuO_2 by O_2 in the reaction mixture in this temperature range. Compared with the Rh/Al_2O_3 system, the interaction of ruthenium dioxide with the alumina surface apparently was much weaker, because the ruthenium dioxide was able to sinter to a particle size providing a measurable intensity in the XRD profile. Sintering may have occurred due to volatilization from well-dispersed ruthenium oxide species, or migration of tiny ruthenium oxide particles over the surface of the alumina support.

The foregoing results of *in situ* Raman and XRD characterizations indicate that in the temperature range before ignition of the POM reaction, the reduction rates of Rh_2O_3 and RuO_2 were lower than the oxidation rates of metallic Rh and Ru, resulting in an oxidized surface. Because CO_2 is the only carbon-containing product for the reaction in this temperature range, it can be concluded that noble metal oxide species (e.g., Rh_2O_3 or RuO_2) are active only for the combustion of CH_4 to CO_2 and H_2O. This is also in agreement with the results reported in the literature.

4.2. Chemical state of the noble metal species in the Rh/Al_2O_3 and Ru/Al_2O_3 catalysts under the POM reaction condition

As the temperature of the sample was increased, the reduction rate of metal oxide by CH_4 [Eq. (2)] increased. When the rate of Eq. (2) exceeded that of Eq. (1), the noble metal oxide species in the catalysts was reduced to the metallic state. With an increasing amount of reduced metal sites, the POM reaction over the catalyst was ignited. The combustion-reforming mechanism (CRR) postulates two reaction zones in the catalyst bed and suggests that synthesis gas is formed via the initially exothermic combustion of CH_4 to CO_2 and H_2O, followed by the endothermic reformation of unconverted CH_4 with CO_2 and H_2O. This reaction scheme requires that most of the metal species in the catalyst near the entrance of the catalyst bed be in oxidized form or that the oxygen coverage on the surface of the metal particles be high enough to catalyze the combustion of CH_4 to CO_2 and H_2O. Previously obtained two-dimensional X-ray absorption spectroscopy (XAS) mapping images on the distribution of Rh^{3+}/Rh^0 species along the Rh/Al_2O_3 [37,39] and $Pt–Rh/Al_2O_3$ [40] catalyst beds under a simulated POM feed ($CH_4/O_2/He = 6/3/91$) at ca. 320 °C are consistent with the CRR scheme.

In contrast to the CRR mechanism, the direct oxidation mechanism (DPO) assumes that H_2 and CO are primary reaction products formed in the zone at the catalyst entrance, where O_2 in the reaction mixture has not been completely consumed. After methane pyrolysis ($CH_4 \rightarrow CH_{xs} + 4\text{-}xH_s$), surface CH_x species react with surface oxygen to CO, and surface hydrogen atoms combine to H_2. This mechanism requires that most of the metal species in the catalyst at the entrance of the catalyst bed be in the reduced form so that methane dissociation to CH_x can occur [12–14,16,19].

The results of *in situ* Raman and XRD characterizations shown in Figs. 5–8 clearly indicate that after ignition of the POM reaction, no Rh_2O_3 or RuO_2 species were detected even in the catalyst located at the top of the catalyst bed, where O_2 was still available in the reaction feed. This means that the noble metal species in the entire catalyst bed were in a highly reduced form under the POM reaction conditions. A sharp axial transition of the catalyst (or noble metal species) from the oxidized state (e.g., Rh^{3+}) to the reduced state (Rh^0), as observed by Grunwaldt et al. [37] and Hannemann et al. [39] on Rh/Al_2O_3 and by Grunwaldt and Baiker [40] on $Pt–Rh/Al_2O_3$ at temperatures slightly above the ignition point of the POM reaction, were not seen under our experimental conditions. This may be because the ignition temperatures for the POM reactions over the Rh/Al_2O_3 catalysts of the present study were between ~430 and ~470 °C, compared with the 330 °C reported by Grunwaldt et al. on their Rh/Al_2O_3 catalyst (prepared by flame spray pyrolysis). The reaction to metallic rhodium, which calls for a relatively high temperature, would proceed preferentially under our experimental conditions, but the amount of oxidized rhodium species in the catalyst at temperatures above 430 °C might be too small to be detected by Raman spectroscopy. To the best of our knowledge, all of the spatially resolved *in situ* XAS characterizations reported to date on catalysts for the POM reaction in which a distinct change in the oxidation state of the active metal species along the catalyst bed was observed were performed at temperatures below 400 °C.

The results of *in situ* Raman characterization on the Rh/Al_2O_3 catalyst are in line with the results of spatially resolved gas species analysis along the catalyst bed reported by Horn et al. [20] for the catalytic partial oxidation of CH_4 on autothermally operated Rh-coated α-Al_2O_3 foams under steady-state conditions. In their experiment, both CO and H_2 were detected in the region near the entrance of the catalyst bed, where O_2 in the reactant had not been completely consumed. Because metallic Rh sites are required for the formation of synthesis gas, it is reasonable to conclude that most of the Rh species located at the front of the Rh-coated α-Al_2O_3 foam catalyst bed also were in the reduced state under the experimental conditions.

On the reduced metal sites, CH_4 can be readily activated by dissociation to surface carbon species (CH_x, $x = 0–3$), which can then convert to CO through a series of surface reactions [6]. In our previous work, Raman bands of surface carbon species (~1330 and ~1570 cm^{-1}) formed by CH_4 dissociation were clearly seen at the entrance of an Ir/SiO_2 catalyst bed under working conditions [41]. For the POM reaction over Rh/Al_2O_3 and Ru/Al_2O_3 catalysts, however, no Raman bands of surface carbon species were detected on the catalysts under similar experimental conditions. This may be due to the higher oxygen coverage on the Rh/Al_2O_3 and Ru/Al_2O_3 catalysts compared with the Ir/SiO_2 catalyst under working conditions. Another possible explanation is that the reactivity of the surface carbon species was higher on Rh/Al_2O_3 and Ru/Al_2O_3 than on the supported Ir catalysts. The Raman bands of the carbon species on Ir/SiO_2 decreased in intensity as the temperature was increased from 500 to 700 °C, and vanished at 750 °C. Further experiments are needed to clarify these questions.

4.3. Comparison of Rh/Al_2O_3 and Ru/Al_2O_3

The results of catalytic performance testing for the reactions over Al_2O_3- and SiO_2-supported catalysts given in Tables 2–4 indicate that the temperatures required to ignite the POM reaction are significantly higher over supported Ru catalysts than over supported Rh catalysts with comparable metal loadings. A similar phenomenon also has been reported for γ-Al_2O_3-supported [38] and MgO-supported [42] Rh and Ru catalysts. On the other hand, the ignition temperatures of the POM reaction over Ru/Al_2O_3-110 and Ru/Al_2O_3-600 catalysts with similar Ru loadings were very close, even though the dispersion of Ru species was much greater in the former (Table 1). These observations suggest that for catalysts with comparable metal loadings, the ignition temperature of the POM reaction is related more to the nature of the noble metal itself than to the dispersion or particle size of the metal species on the support.

The foregoing results of *in situ* Raman and XRD characterizations clearly indicate that the noble metal species in the catalysts were in the fully oxidized state before ignition of the POM reaction. On the oxidized metal surface, the reaction between CH_4 and O_2 occurs via the Eley-Rideal mechanism; that is, CH_4 in the gas phase (or weakly adsorbed) reacts with strongly adsorbed or lattice oxygen [43]. This suggests that the ignition temperature of the POM reaction should be closely related to the metal–oxygen (M–O) bond strength of the metal oxides. M–O species with higher bond strength are less reactive, and thus higher temperatures are needed to initiate their reaction with CH_4. The temperature gap between the ignition temperatures of supported Rh and Ru catalysts can be rationally explained by the significant differences in the Rh–O and Ru–O bond strengths. The bond strength of Ru–O (481 ± 63 kJ/mol) is much higher than that of Rh–O (377 ± 63 kJ/mol) [44]. This should result in a more difficult reduction of ruthenium oxide than of rhodium oxide under the POM reaction atmosphere. A linear relationship between the ignition temperatures and M–O bond strengths also has been reported for reactions of a C_2H_6/air mixture over Pt, Pd, Rh, and Ir foils [45].

Once the POM reaction is ignited, most of the metal species in the Rh/Al_2O_3 and Ru/Al_2O_3 catalysts are in the reduced state. The reaction of CH_4 with O_2 occurs through the Langmuir–Hinshelwood mechanism, in which adsorbed CH_4 and O_2 species react with one another [43]. Normal (>1) deuterium isotope effects on CH_4 conversion (or CH_4 consumption rate) and CO yield (or CO formation rate) have been reported for the POM reaction on supported Rh catalysts [26,46] and Ru catalysts [47] at 550–

700 °C. This suggests that the dissociation of CH_4 to CH_x species or the formation of CO involving cleavage of a C–H bond is a slow or rate-determining step that controls the overall process. Under these circumstances, the reaction of surface carbon species with adsorbed oxygen may be a fast step, and the formation of primary products (CO or CO_2) may depend mainly on the oxygen coverage on the metal surface. Higher oxygen coverage is more readily obtained on metals with greater M–O bond strength or a higher affinity for oxygen. This is in line with the results of our CH_4 pulse reaction experiments shown in Fig. 9. As mentioned in Section 2 because the catalysts used in the pulse reaction experiments were prereduced with H_2 at 600 °C, the source of the oxygen responsible for the reoxidation of metallic Rh and Ru species in the catalysts between two CH_4 pulses should be mainly the O_2 in the He flow. Due to the greater bond strength of Ru–O compared with Rh–O, the reduced Ru species will be more easily oxidized by the O_2 in the carrier gas than the reduced Rh species. As a result, the oxygen coverage on the surface of reduced ruthenium catalysts (Ru powder or Ru/Al_2O_3) between two CH_4 pulses will be sufficiently high to oxidize CH_4 to both CO_2 and CO, whereas the oxygen species on the Rh powder or supported Rh catalysts will favor the formation of CO only, because its concentration on the catalyst surface under the same experimental conditions is too low to completely oxidize the CH_4 to CO_2. Thus, it can be rationally concluded that for the POM reaction carried out under similar experimental conditions, the oxygen coverage will be higher on the surface of Ru/Al_2O_3 than on the surface of Rh/Al_2O_3. This suggests that Rh/Al_2O_3 is a better catalyst than Ru/Al_2O_3 for promoting the POM reaction via the direct partial oxidation pathway.

5. Conclusion

Based on the results of our *in situ* Raman and XRD characterizations and catalytic performance tests on the Rh/Al_2O_3 and Ru/Al_2O_3 catalysts, we can conclude that, at temperatures below the ignition point of the POM reaction, the noble metal species in both catalysts (at least those on the surface of the metal particles) were in the fully oxidized form. The oxidized metal species were active only for the complete oxidation of CH_4 to CO_2 and H_2O. Most of the noble metal species in the catalysts changed from the oxidized form to the metallic state at the start of the POM reaction. At temperatures above the ignition point of the POM reaction, the catalyst was in a highly reduced state. The amount of Rh_2O_3 or RuO_2 in the catalyst at the entrance of the catalyst bed (where O_2 was still available in the reaction mixture) was below the detection level of Raman spectroscopy. Because of the greater M–O bond strength of Ru–O compared with Rh–O, the Ru/Al_2O_3 catalyst showed a greater tendency toward oxidation and was more difficult to reduce than the Rh/Al_2O_3 catalyst under the $CH_4/O_2/Ar$ mixture at the POM stoichiometric ratio ($CH_4/O_2 = 2$). These factors affect the coverage of oxygen species on the surface of the Rh/Al_2O_3 and Ru/Al_2O_3 catalysts under the POM reaction conditions and, consequently, affect the reaction pathways of synthesis gas formation over these two catalysts.

Acknowledgments

This project was supported by the Ministry of Science and Technology of China (2005CB221401), the National Natural Science Foundation of China (20433030 and 20423002), the Key Scientific Project of Fujian Province, China (2005HZ01-3), and the Natural Science Foundation of Fujian Province, China (2007J0168).

References

[1] J.R. Rostrup-Nielsen, Catal. Today 18 (1993) 305.
[2] A.T. Ashcroft, A.K. Cheetham, M.L.H. Green, P.D.F. Vernon, Nature 352 (1991) 225.
[3] D.A. Hickman, L.D. Schmidt, Science 259 (1993) 343.
[4] A.P.E. York, T.C. Xiao, M.L.H. Green, Top. Catal. 22 (2003) 345.
[5] Y.H. Hu, E. Ruckenstein, Adv. Catal. 48 (2004) 297.
[6] D.A. Hickman, L.D. Schmidt, J. Catal. 138 (1992) 267.
[7] M. Prettre, Ch. Eichner, M. Perrin, Trans. Faraday Soc. 42 (1946) 335.
[8] I. Tavazzi, A. Beretta, G. Groppi, P. Forzatti, J. Catal. 241 (2006) 1.
[9] F. van Looij, E.R. Stobbe, J.W. Geus, Catal. Lett. 50 (1998) 59.
[10] J.C. Slaa, R.J. Berger, G.B. Marin, Catal. Lett. 43 (1997) 63.
[11] D. Dissanayake, M.P. Rosynek, K.C.C. Kharas, J.H. Lunsford, J. Catal. 132 (1991) 117.
[12] O.V. Buyevskaya, D. Wolf, M. Baerns, Catal. Lett. 29 (1994) 249.
[13] E.P.J. Mallens, J.H.B.J. Hoebink, G.B. Marin, J. Catal. 167 (1997) 43.
[14] K.H. Hofstad, J.H.B.J. Hoebink, A. Holmen, G.B. Marin, Catal. Today 40 (1998) 157.
[15] M. Fathi, F. Monnet, Y. Schuurman, A. Holmen, C. Mirodatos, J. Catal. 190 (2000) 439.
[16] D. Wang, O. Dewaele, A.M. De Groote, G.F. Froment, J. Catal. 159 (1996) 418.
[17] W.Z. Weng, Q.G. Yan, C.R. Luo, Y.Y. Liao, H.L. Wan, Catal. Lett. 74 (2001) 37.
[18] W.Z. Weng, M.S. Chen, H.L. Wan, Chem. Rec. 2 (2002) 102.
[19] Y.H. Hu, E. Ruckenstein, J. Phys. Chem. A 102 (1998) 10568.
[20] R. Horn, K.A. Williams, N.J. Degenstein, L.D. Schmidt, J. Catal. 242 (2006) 92.
[21] W.Z. Weng, X.Q. Pei, J.M. Li, C.R. Luo, Y. Liu, H.Q. Lin, C.J. Huang, H.L. Wan, Catal. Today 117 (2006) 53.
[22] A.C. Yang, C.W. Garland, J. Phys. Chem. 61 (1957) 1504.
[23] F. Solymosi, M. Pásztor, J. Phys. Chem. 89 (1985) 4789.
[24] M.I. Zaki, G. Kunzmann, B.C. Gates, H. Knözinger, J. Phys. Chem. 91 (1987) 1486.
[25] P. Basu, D. Panayotov, J.T. Yates Jr., J. Phys. Chem. 91 (1987) 3133.
[26] H.Y. Wang, E. Ruckenstein, J. Phys. Chem. B 103 (1999) 11327.
[27] D. Dissanayake, M.P. Rosynek, J.H. Lunsford, J. Phys. Chem. 97 (1993) 3644.
[28] C.P. Hwang, C.T. Yeh, Q. Zhu, Catal. Today 51 (1999) 93.
[29] H.C. Yao, S. Japar, M. Shelef, J. Catal. 50 (1977) 407.
[30] H. Madhavaram, H. Idriss, S. Wendt, Y.D. Kim, M. Knapp, H. Over, J. Aßmann, E. Löffler, M. Muhler, J. Catal. 202 (2001) 296.
[31] P. Betancourt, A. Rives, R. Hubaut, C.E. Scott, J. Goldwasser, Appl. Catal. A Gen. 170 (1998) 307.
[32] I. Balint, A. Miyazaki, K. Aika, J. Catal. 207 (2002) 66.
[33] M. Boudart, J. Mol. Catal. 30 (1985) 27.
[34] C.T. Williams, C.G. Takoudis, M.J. Weaver, J. Phys. Chem. B 102 (1998) 406.
[35] S.Y. Mar, C.S. Chen, Y.S. Huang, K.K. Tiong, Appl. Surf. Sci. 90 (1995) 497.
[36] J.D. Grunwaldt, L. Basini, B.S. Clausen, J. Catal. 200 (2001) 321.
[37] J.D. Grunwaldt, S. Hannemann, C.G. Schroer, A. Baiker, J. Phys. Chem. B 110 (2006) 8674.
[38] S. Rabe, T.B. Truong, F. Vogel, Appl. Catal. A Gen. 292 (2005) 177.
[39] S. Hannemann, J.D. Grunwaldt, N. Van Vegten, A. Baiker, P. Boye, C.G. Schroer, Catal. Today 126 (2007) 54.
[40] J.D. Grunwaldt, A. Baiker, Catal. Lett. 99 (2005) 5.
[41] W.Z. Weng, C.R. Luo, J.M. Li, Y. Liu, H.Q. Lin, C.J. Huang, H.L. Wan, Acta Chim. Sinica 62 (2004) 1853.
[42] D. Qin, J. Lapszewicz, X. Jiang, J. Catal. 159 (1996) 140.
[43] Y.H. Hu, E. Ruckenstein, J. Phys. Chem. B 102 (1998) 230.
[44] R.C. Weast, M.J. Astle (Eds.), CRC Hand Book of Chemistry and Physics, 62nd ed., CRC Press Inc., Boca Raton, FL, 1981–1982, F-184.
[45] G. Veser, M. Ziauddin, L.D. Schmidt, Catal. Today 47 (1999) 219.
[46] C.T. Au, H.Y. Wang, J. Catal. 167 (1997) 337.
[47] C. Elmasides, X.E. Verykios, J. Catal. 203 (2001) 477.